

Solar evaporation of a hanging plasmonic droplet

Guohua Liu^a, Hui Cao^a, Jinliang Xu^{b,*}

^a Key Laboratory of Condition Monitoring and Control for Power Plant Equipment of Ministry of Education, North China Electric Power University, Beijing 102206, China

^b Beijing Key Laboratory of Multiphase Flow and Heat Transfer for Low Grade Energy Utilization, North China Electric Power University, Beijing 102206, PR China



ARTICLE INFO

Keywords:

Solar energy
Droplet evaporation
Plasmonic nanoparticles
Collective heating

ABSTRACT

Plasmonic nanoparticles attract great attention owing to their strong light-to-heat conversion properties. Fundamental understanding of their photothermal performance is critical to develop solar-to-heat systems. Here, we use gold nanoparticles as the photothermal agent. Solar water evaporation are explored through a hanging droplet containing the nanoparticles. These nanoparticles induce multiple scattering events, increasing photon absorption and concentrating the light within the mesoscale domain, leading to an intense collective heating that trigger the evaporation. The droplets with different initial-particle-concentrations lead to evaporation at various rates (e.g. K constant in D²-law), and an optimal initial-particle-concentration can be expected. With steam releasing from the surface, shrinking of the droplet increases the particle concentration in the domain that accelerates the surface evaporation. The surface evaporation rate increases with the increasing concentration of nanoparticle, reaching an optimized value at a threshold concentration and then stable. K values demonstrate a nonlinear dependence over the time, reflecting complex heat-transfer physics behind the phenomenon. We assume that the collective heating is controlled by two parameters: one that relates the morphology properties of the droplet and the other that characterizes the gap between nanoparticles. This work provides an important insight on the evaporation dynamics of plasmonic droplets, and stands for a basis to design the plasmonic solar heating systems.

1. Introduction

Solar water evaporation is an important process in many industries, such as power generation, absorption chillers, medical and waste sterilization, water purification and desalination systems, etc. (Gao et al., 2016; John A. Duffie; Kalogirou, 2004; Lewis, 2016; Liu et al., 2017; Neumann et al., 2013a; Shang and Deng, 2016; Thirugnanasambandam et al., 2010). The current technologies rely on absorbing solar energy through macroscopic cavity or vessel surface and transferring the heat into the surrounding media and thus suffer from energy loss from the absorbing surface to bulk fluid. High optical concentration are normally used to overcome the inefficiencies (Weinstein et al., 2015). However, this adds complexity and cost to the solar thermal system. Alternative strategies are proposed to use solar energy under a moderate intensity, for example, directional selectivity of the radiation by spectrally selective vessel inner walls achieving a efficiency of 75% without high heat fluxes (Weinstein et al., 2014). Other examples introduce carbon nanofluids (Deng et al., 2017; Loeb et al., 2018; Wang et al., 2016) or porous graphene materials to assist water evaporation, demonstrating solar thermal efficiencies above 45 or 80% respectively, due to their broadband absorption in the solar spectrum (Chen et al., 2017; Ghasemi

et al., 2014; Li et al., 2016).

Despite of the above approaches, a highly active surface of metal nanoparticles in a volumetric dispersion can be engineered to locally enhance the evaporation. The volumetric absorbers ranging from plasmonic porous membranes, biomaterial aerogels to gas-particle suspensions and nanofluids have been reported to reduce surface temperatures (Bertocchi et al., 2004; Lenert and Wang, 2012; Neumann et al., 2013b; Otanicar et al., 2010; Tian et al., 2016; Zhou et al., 2016; Zhu et al., 2017). Among which, the plasmonic nanofluid is an attractive route for steam generation since it can implement easily and enhance critical heat flux in certain boiling condition (Deng et al., 2017; Jin et al., 2016b; Kim et al., 2007; Liu et al., 2006; Loeb et al., 2018; Lombard et al., 2014; Neumann et al., 2013a). Different mechanisms have been proposed for understanding the underlying physics. Earlier studies focus on vapor nucleation around the nanoparticles (Fang et al., 2013; Lombard et al., 2014; Neumann et al., 2013b; Zielinski et al., 2016). They hold that the initial vapor expand and coalesce to produce micro-bubbles that can be further released at air-water interface. However, the nanobubble is unlikely to occur under normal radiation because that only can be observed under intensive laser heating (Baffou et al., 2014; Lombard et al., 2017; Metwally et al., 2015; Wang, Y. et al.,

* Corresponding author.

E-mail address: xjl@ncepu.edu.cn (J. Xu).

2017). Other research claim that the global temperature rising in nanofluids by collective heating is the key mechanism (Baral et al., 2014; Govorov and Richardson, 2007; Ni et al., 2015; Richardson et al., 2009). While non-linearly decay of optical depth in nanofluid undoubtedly results in temperature difference (Khullar et al., 2014; Lee et al., 2012). Recent studies assume that an intense localized heating under focal area induces the evaporation, albeit considerable non-uniform temperature exist within the liquid (Amjad et al., 2017; Hogan et al., 2014; Jin et al., 2016a; Jin et al., 2016b; Wang, X. et al., 2017). For such cases, it is difficult to control the heat diffusion under sub-cooled condition as that represents a mixture of material properties and fluid transport (Baffou et al., 2010; Berry et al., 2015; Roxworthy et al., 2014). Obviously, a better understanding on solar evaporation of plasmonic nanofluids is highly demanded.

In this paper, we propose a nano/mesoscale engineering concept that combines the plasmonic properties of nanoparticles and the extended active surface provided by mesoscale droplet to boost solar vapor generation. A set of experiments are performed on photoheating of a water droplet containing gold nanoparticles. Key elements such as temperature and morphology evolution of the droplet are traced to understand the evaporation dynamics. A four-stage heating scenario has been identified based on the results. The highlights of this work are (i) localizing the light energy into the mesoscale domain by both scattering and absorption that leads to a collective photoheating, (ii) providing the small fluid volume to minimize the temperature difference and the large surface area for steam generation and escape, (iii) demonstrating a detailed picture on the evaporation process of plasmonic droplet. These studies will be useful for application of this unique phenomenon.

2. Materials and methods

2.1. Gold nanofluids

Gold chloride hydrate (HAuCl_4 , Au \geq 49%) solution and aqueous tri-sodium citrate ($\text{Na}_3\text{C}_6\text{H}_5\text{O}_7$, 99.8%) were purchased from Sigma-Aldrich and used as received. Deionized water was used throughout the experiments. Gold nanoparticles generally can be synthesized by the citrate reduction method, the Brust-Schiffrin and the modified Brust-Schiffrin method (Zhao et al., 2013). In our experiment, the synthesis of gold nanoparticles followed by the citrate reduction method (Ji et al., 2007; Jin et al., 2016b). Specifically, gold chloride hydrate solution was mixed with trisodium citrate solution. The mixture was then heated to boiling temperature until its color shift to wine red. After sonication and aged, the resultant was last purified by a membrane dialysis method. The obtained nanofluids present good stability and can be further used for our experiments by diluting it into the required concentration.

2.2. Experimental setup

Fig. 1a shows a setup image of the experiment. The main apparatus consist of (1) data acquisition model (Yokogawa DL750), (2) synchronization hub, (3) computer, (4) Xenon lamp (CEL-S500), (5) thermocouple tip (Omega TT-T-36), (6) high speed camera with a micro-focal lens (IDT Motion Pro Y4 model, MP-E65mm lens), (7) glass cloak, (8) thermocouple wire, and (9) four-axis positioning guide. The thermocouple positioned on an iron beam (Fig. 1b is the circled part in Fig. 1a) that is linked with the positioning guide to precise control of the distance between the couple tip and the light source. The thermocouple has wire diameter of 0.12 mm and a tip diameter of 0.40 mm with a response time of 50 ms, pinned into the droplet center (Fig. 1c). The thermocouple with data acquisition model was used to measure the droplet temperature at a frequency of 5 Hz. The high-speed camera captured the images through hole 1 at speed of 10 Hz. The synchronization hub connected to computer was introduced to synchronize the

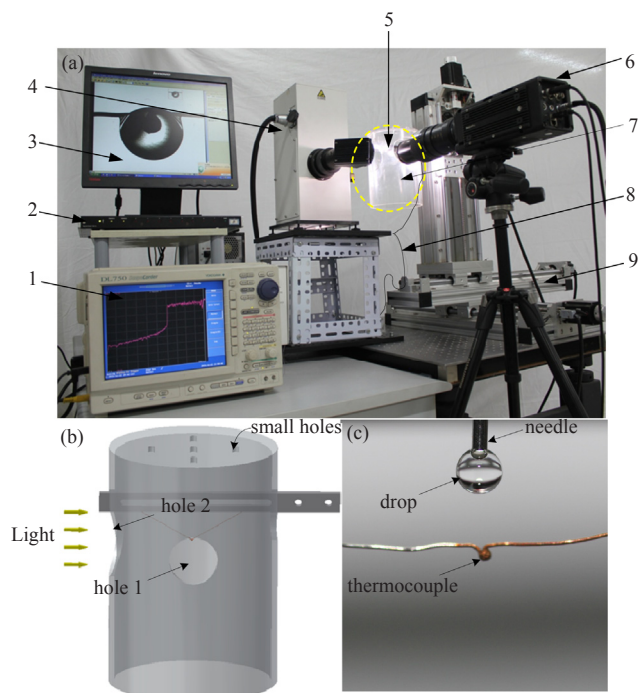


Fig. 1. The experimental setup (a) (1) data acquisition model, (2) synchronization hub, (3) computer, (4) Xenon lamp, (5) thermocouple tip, (6) high speed camera with a micro-focal lens, (7) glass cloak, (8) thermocouple wire, and (9) four-axis positioning guide. (b) A schematic diagram of the circled part in Fig. 1a. (c) A close-up image of the couple tip and the droplet.

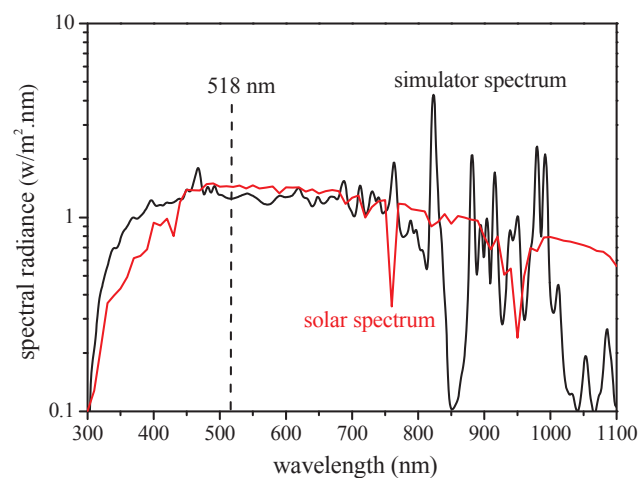


Fig. 2. Simulated spectrum offered by Xenon lamp with an AM1.5 filter versus solar spectrum.

both systems, and their acquisition duration was set to 20 min for each experiment. The light spectrum offered by Xenon lamp with an AM1.5 filter was resembled to the solar spectrum in visible range of 300–800 nm (Fig. 2), which therefore can be used as the simulated solar source.

2.3. Experiment procedure

Evaporation experiments were conducted in batch under irradiation on calm sunny days. The xenon lamp run for 15 min before the experiment to achieve a stable intensity. Then the intensity was quantified by an optical power meter (NP2000). A knob of xenon lamp was used to adjust the intensity at 1200 W/m^2 , and then the light output was shut with an opaque shade. The diluted nanofluids were sonicated for 5 min

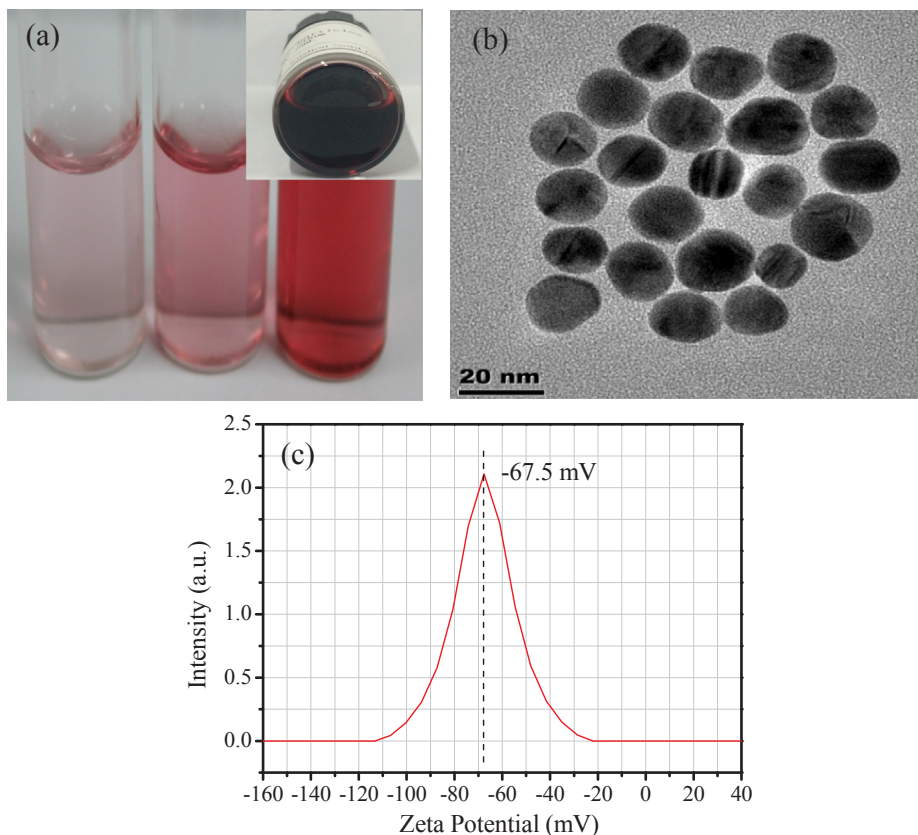


Fig. 3. Characterization of gold nanofluids (a) image of gold nanofluids at different concentrations with an inset image of the as-prepared gold nanofluid. (c) TEM image of the gold nanoparticles and (d) zeta potential graph.

before loaded it into the syringe. Droplets with a diameter ~ 1.5 mm were produced by a contact angle measuring instrument (OCA15plus, Dataphysics, Germany) and can be quickly hung on the thermocouple tip. The glass cloak enveloped the hanging droplet for evaporation. The synchronizer triggered the camera as well as the data acquisition system to record the data and images. The solar evaporation was running after removing the shade. The uncertainty in temperature measurement was about 0.25 K and in evaluation of the droplet diameter was about 1.5%.

3. Results and discussion

3.1. Characterization of gold nanofluids

Fig. 3a presents an image of the diluted solutions at different concentrations e.g. $\sim 10, 25, 100$ $\mu\text{g/ml}$, with an inset photographic image of the initial nanofluid (~ 1 mg/ml). The shape and size of gold nanoparticles are characterized by a transmission electron microscopy (TEM-JEOL 2011). The high-resolution image shows the excellent dispersion and quasi-spherical morphology of gold nanoparticles (Fig. 3c). The nanoparticle diameter is evaluated by analyzing a number of particles with software. The mean diameter is determined as 16 nm with a relative standard deviation of 8.6%. The zeta potential of the gold nanofluid is about -67.5 mV (Fig. 3d), further supporting a good stability of the suspension.

Optical properties of the nanofluids were examined by UV–vis spectrometry (UV3600), where the nanofluid was held in quartz cuvettes with a 10 mm beam path length and the reference fluid was DI water. As shown in Fig. 4a, due to the strong surface plasmon resonance effect of the gold nanoparticles in visible light range, an obvious absorption peak is found at the wavelength of 518 nm for all the suspensions. Such peak is consistent with the result of spherical gold

nanoparticles with the size of ~ 16 nm (Guo et al., 2017; Jain et al., 2006). The absorption coefficient of plasmonic nanofluids at 518 nm increases with the particle concentration. A linear relationship exists between the absorbance and the concentration of gold nanofluids according to the Beer-Lambert Law (Swinehart, 1962). The transmittance of gold nanofluids decrease with the increase of particle concentration (Fig. 4b). The deionized water almost not absorb sunlight during the visible range and its transmittance is approximately 90%. While the transmittance of plasmonic nanofluids gradually decreasing as the concentration increase, it is only about 10% for the nanofluid at 100 $\mu\text{g/ml}$.

3.2. Solar evaporation of the droplet

The diffusion-controlled approach is commonly used to describe the evaporation process of a droplet. When the liquid-vapor interface is in thermodynamic equilibrium, the rate of droplet evaporation is equal to the rate of mass diffusion at any given moment. The evaporation rate can be expressed as $-\frac{dm}{dt} = 4\pi R_s D_v \frac{M}{RT} (P_s - P_\infty)$. (Sadek et al., 2014) Where R_s is the droplet radius, D_v the diffusion coefficient of vapor in air, M the molecular weight, T the temperature, R the gas constant, P_s the partial pressure at the surface, and P_∞ the infinite partial pressure. Therefore, the evaporation rate of droplet is a function of the radius, the temperature, the partial pressure, and the transport properties of the air surrounding of the droplet. The initial conditions are controlled in our experiments. Size of the droplets are $\sim 1.76, 1.78, 1.76$ and 1.80 mm^3 . Environment conditions are monitored as temperature of 19.4, 19.2, 18.9, 18.7 $^\circ\text{C}$, humidity of 40%, 32%, 42.2%, 35.4% and pressure of 102.1, 102.2, 101.6 and 101.2 kPa. The partial pressure of water vapor thus can be calculated as 43.1, 40.9, 32.5 and 35.8 kPa, correspondingly.

Fig. 5a shows temperature traces of the base water droplet and the

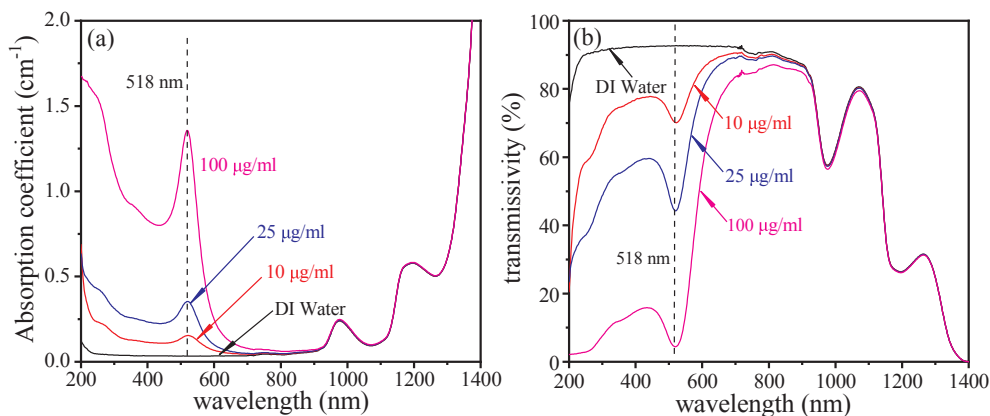


Fig. 4. (a) Absorption coefficient and (b) transmission spectrum of the plasmonic nanofluids at different concentrations.

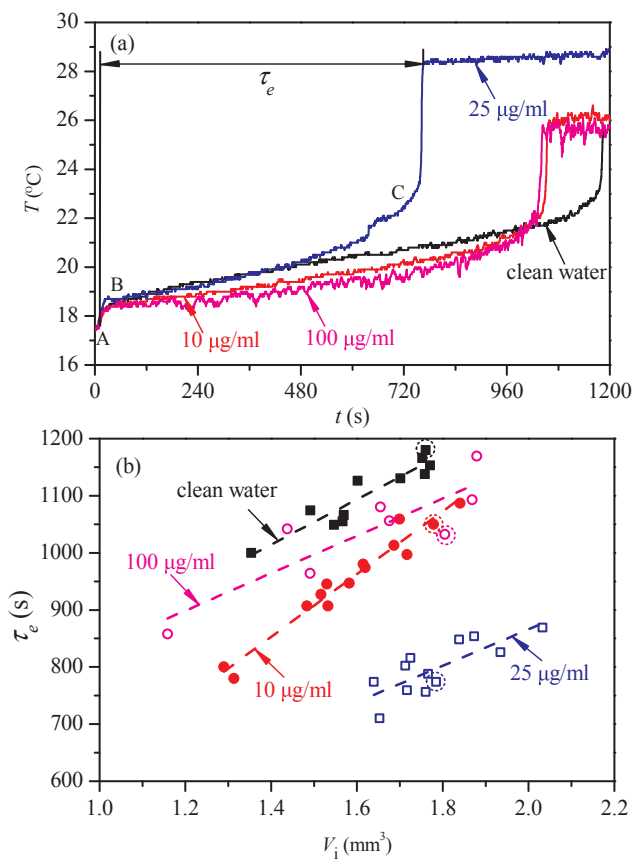


Fig. 5. (a) Temperature profiles for the evaporation of a water droplet and nanofluid droplets at various concentrations. (b) Evaporation duration versus initial volume of the droplet.

plasmonic droplets. It can be seen that there are two heating phases on the temperature profiles: (1) transient heating phase (A-B), in which the droplets absorbing solar energy and its temperature rapidly increase to the wet-bulb temperature. (2) quasi-equilibrium evaporation phase (B-C), shrinkage of the droplet due to evaporation and the droplet temperature is slowly heating up. The transient heating phase is relative short compared to the quasi-equilibrium evaporation stage. All the temperature traces exhibit the same trend, but the evaporation rates are different. The evaporation duration τ_e represents the time consuming by rising the droplet temperature from its initial temperature to the sharp increasing of temperature at end of evaporation. We observe that the evaporation duration of the base water droplet is about 1180 s, while the plasmonic droplet at 25 $\mu\text{g/ml}$ only requires ~ 757 s to end

the evaporation at a high temperature. The evaporation time of the droplets at 10 and 100 $\mu\text{g/ml}$ are 1050 s and 1030 s, respectively. Clearly, the evaporation process of plasmonic droplets is generally faster than that of the pure water. This is because water does not absorb the visible light energy, while the gold nanofluids significantly absorb the energy due to surface plasmon effect. We also noted that the temperature profiles of plasmonic droplets at 10 and 100 $\mu\text{g/ml}$ is slightly lower than that of the water droplet during the heating stage. This can be explained that more energy is paid to latent-heat evaporation since the plasmonic droplets have a fast evaporation rate.

At initial evaporation, only independent multi-scattering occurs and interparticle gap does not play role in the absorption. The photo-heating effect of droplets are increased with the increasing of initial concentration. While as the evaporation proceeding, the particles within droplets would agglomerate sooner or later. The droplet at 100 $\mu\text{g/ml}$ agglomerates much earlier on part of its surface than that of the others due to its high concentration. The resulting nanoparticle clusters at interface promote electron tunneling between the particles and reduce the intensity of local electrical field. Moreover, back scattering effect due to the clusters is dominated at air/water interface. An neglectable part of light is scattered back to the air, which leads to the decrease of temperature of the solution. Therefore, we assume the plasmonic droplet at 25 $\mu\text{g/ml}$ has an optimal initial-interparticle-gap to enable strong solar-to-heat conversion for supporting both latent heat of evaporation and sensible heat of the increased temperature (Ghosh and Pal, 2007; Hentschel et al., 2010; Jain et al., 2007). The increased temperature is thus higher than that of pure water or 10 $\mu\text{g/ml}$ case.

Fig. 5b is a diagram of the evaporation time versus the initial volume of droplet. The data points are the experiments carried out and the dotted line is the fitting result of the data. It can be seen that the bigger is the droplet volume, the longer is the evaporation duration, which is consistent with the D^2 -law (Chen, R.-H. et al., 2010; Langmuir, 1918). From the data, we noticed that the relative fitting error of the plasmonic droplets increases with the increasing particle concentration, which presents a large deviation than that of the base water droplet. This is due to the droplet at high particle concentration has a strong evaporation rate that induces complex heat and mass transfer to enhance the Brown movement, thus resulting in unstable floating of the experimental data.

Fig. 6 is snapshots of the evaporating droplets. The initial size of droplets is well-controlled at ~ 1.50 mm. The thermocouple tip pins in the droplet center throughout the experiment. It can be seen that the droplet at 25 $\mu\text{g/ml}$ appears a fastest drying process and completes evaporation at 720 s (Fig. 6b). However, the evaporation duration of the base water droplet extends to ~ 1080 s (Fig. 6a), which consumes almost 1.5 times of the time than that of the droplet at 25 $\mu\text{g/ml}$. These observations are consistent with the temperature results. Moreover, the

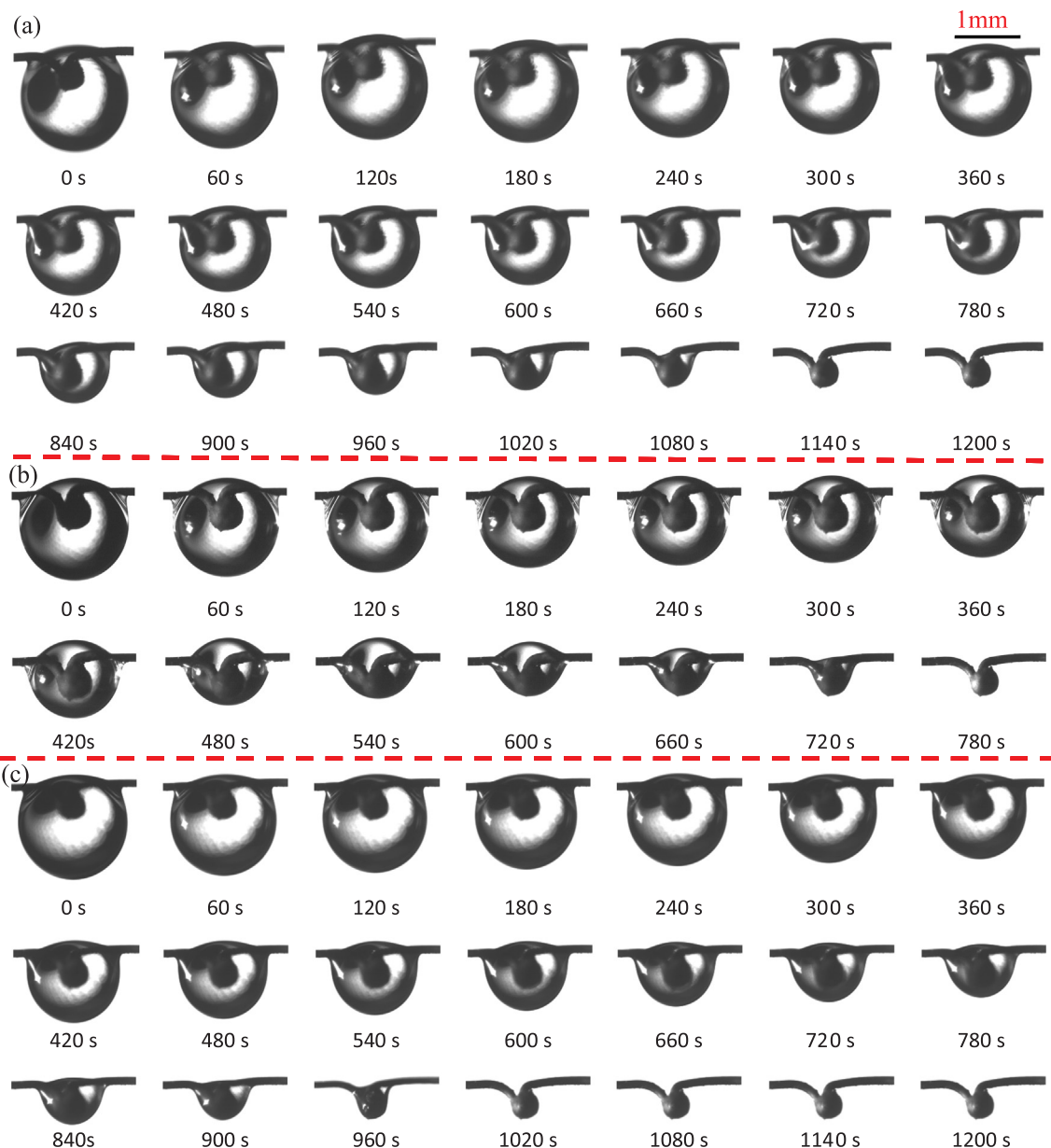


Fig. 6. Successive images of the evaporating droplet with (a) deionized water, and gold nanofluids at concentration of (b) 25 and (c) 100 ug/ml.

morphology of plasmonic droplet presents a quasi-ellipsoid shape as evaporation proceeding. While that of the base water droplet exhibits a spherical shape. This difference may be come from the difference of the apparent surface tension on the evaporating droplets (Chen et al., 2011).

Fig. 7 presents the images and corresponding models for an initial droplet and a plasmonic droplet under evaporation. The mass of initial droplet is larger than the evaporating droplet due to the steam releasing reduces the mass ($m < m_i$), while the tension attached to the thermocouple wire is quasi-constant as σ . So the whole action of the forces tending to achieve a balance on the droplet and that gives rise to $\theta > \theta_i$, thus presenting an ellipsoid shape. To quantify the physical parameters, D_x and D_y are defined as the lateral and longitudinal diameter of the droplet, respectively. Hereby, the droplet volume can be calculated as $V = \frac{\pi}{6}(D_x D_y^2 - d^3)$, the droplet surface area $A = S_{ellipsoid} = \pi(D_y^2 + 2D_x D_y) = S_{sphere} = 4\pi D^2$ and the equivalent diameter $D^2 = (D_y^2 + 2D_x D_y)/4$, where d is the tip diameter of thermocouple. To determine the mass loss, density of the loss volume can be set at a density of water $\sim 1000 \text{ kg/m}^3$ since the nanoparticles do not escape

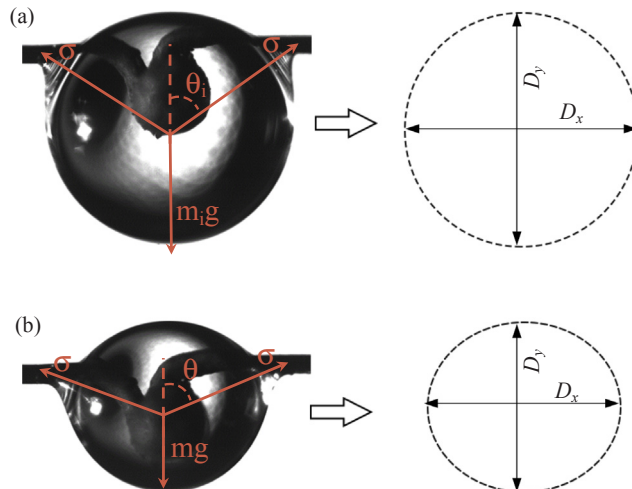


Fig. 7. Images and the models for (a) the initial and (b) the evaporating droplet.

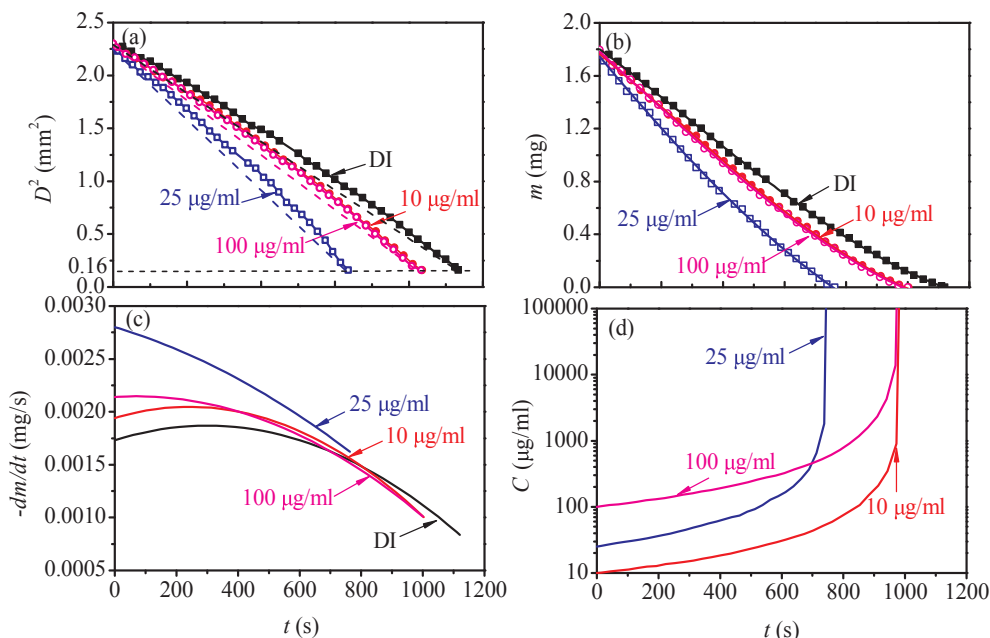


Fig. 8. Transient parameters during the evaporation process. (a) D^2 , (b) the mass of droplet, (c) the evaporation rate and (d) the particle concentration within the droplet as a function of time.

from the droplet with the produced steam. Hereby, transient droplet mass can be evaluated as $m = \rho V = \rho \frac{\pi}{6} (D_x D_y^2 - d^3)$. The mass data then can be fitted as a cubic function versus time, and thus we can obtain the evaporation rate by deriving the function. The transient particle concentration dynamic changes with steam releasing. Following the mass-conservation law, we calculate the transient particle concentration as $c = c_o m_o / m$, where c_o , m_o are the initial concentration and the droplet mass.

Fig. 8 shows the transient physical parameters including D^2 , the droplet mass, the evaporation rate as well as the transient particle concentration. The evaporation constant is defined as $K = (D_o^2 - D_t^2) / t$, where D_o is the initial droplet diameter and D_t is the transient droplet diameter. According to the above formula, the mean evaporation constants of the droplet with base water, 10, 25 and 100 $\mu\text{g/ml}$ nanofluids are 1.90×10^{-3} , 2.12×10^{-3} , 2.76×10^{-3} and $2.14 \times 10^{-3} \text{ mm}^2/\text{s}$, respectively. The evaporation constant of droplet at 25 $\mu\text{g/ml}$ is the largest one that is consistent with the temperature result. More importantly, as the evaporation proceeds, K values of plasmonic droplet exhibit non-linear properties over time that causing deviation from the classical D^2 -law for pure fluid droplet evaporation (Chen, R.-H. et al., 2010; Chen et al., 2011). This is because the droplets not only absorb heat from the surrounding medium but also generate volumetric heat by themselves when exposed to light. Fig. 8b indicates the mass loss over time. The mass losing rate is slowly decreased as the evaporation progress. Fig. 8c presents the evaporation rate of the droplets. The rate decreasing slowly is due to the reducing the effective liquid surface area for both light harvesting and evaporation, which is consistent with the mass loss result. Fig. 8d shows the particle concentration profiles depending on the thermal conditions and aggregation kinetics, and that tends to be infinity at end of evaporation due to dry out. For this transition, Peclet number, a non-dimensional ratio of particle diffusion time to the droplet lifetime, and initial particle concentration possible play an important role (Wei et al., 2016).

Plasmonic droplet evaporation is a uniform process for solar energy utilization because the particle concentration of the nanofluid as well as the surface evaporation rate is dynamic varying with the time. The surface evaporation rate ($K_o = \frac{dm}{dt} / A$) as a function of the particle concentration is presented in Fig. 9. It shows that as the concentration increases, the surface evaporation rate first increases steadily, achieving

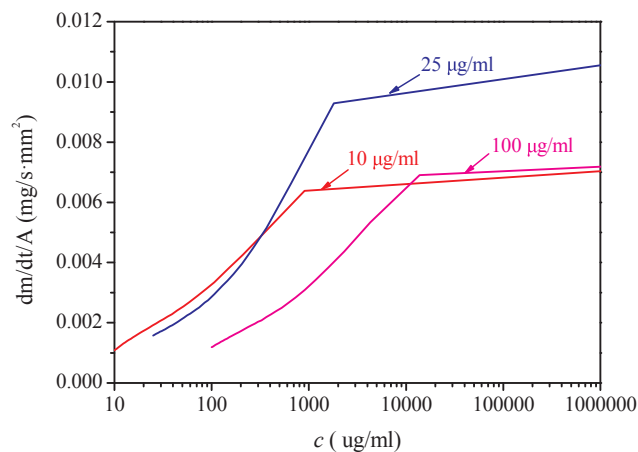


Fig. 9. Surface evaporation rate versus the particle concentration as shrinking of the droplets due to evaporation.

a threshold value and then remains stable. The droplet at 25 $\mu\text{g/ml}$ reaches an optimized rate at the concentration of $\sim 900 \mu\text{g/ml}$. The optimized concentration of 10 and 100 $\mu\text{g/ml}$ droplets are ~ 1800 and $\sim 13500 \mu\text{g/ml}$, correspondingly. These optimum values maybe correspond to a certain critical point before crushing of the droplet.

3.3. Physical evolution and heating mechanism

Evaporation of plasmonic droplets is a complex process in consideration of not only liquid-side diffusion and gas-side heat and mass transfer, but also light-to-heat transformation as well as aggregation as a particulate process (Chen, H. et al., 2010; Deegan et al., 1997; Gerken et al., 2014; Ming et al., 2008; Roxworthy et al., 2014). The removal of moisture from a plasmonic droplet involves simultaneous phase change phenomena, heat and mass transport, and the process is coupled to concurrent particle movement within the droplet. Both the evaporation rate and particle concentration depend upon the air temperature, humidity, pressure, light source intensity and the transport properties, in addition to the initial temperature and diameter of the droplet. Based

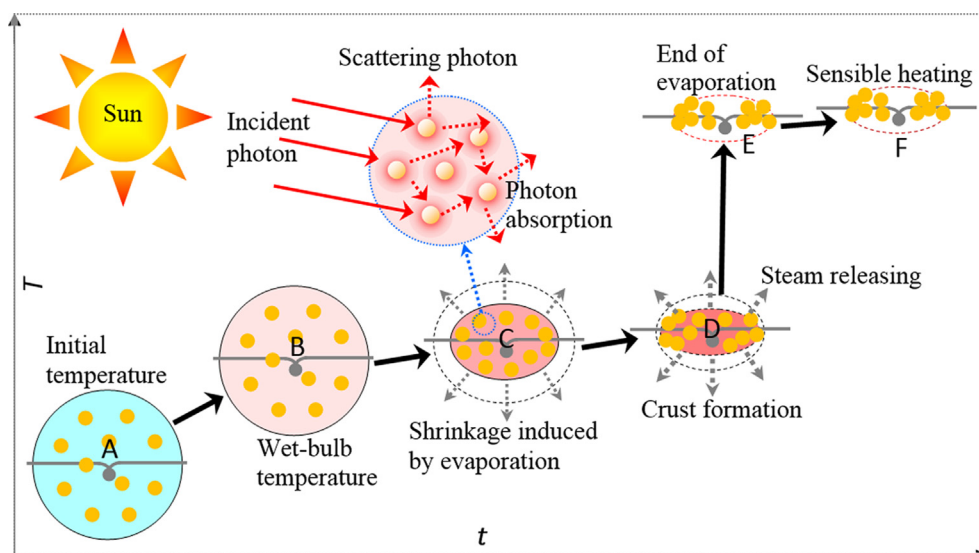


Fig. 10. Heating road map and mechanism. A collective heating mechanism mediated by both light scattering and absorption. A-B sensible heat, B-D shrinkage with a strong surface evaporating rate, D-E crust progressing, E-F sensible heat.

on our observation, we propose a four-stage heating scenario for the plasmonic droplets (Fig. 10). In the first stage (A-B), the droplet is subjected to light irradiation and flow of air steams, gains sensible heat, and the temperature rapidly increase to wet-bulb temperature. Then the droplet at wet-bulb temperature is evaporated at a quasi-constant rate (B-D). This excess liquid evaporation results in droplet diameter shrinking and simultaneous increase of particle concentration within the droplet, thus can harvest more solar energy to accelerate the surface evaporation rate. At end of this stage, the strong local evaporation leads to the precipitation of solid fraction on the interface of droplet/thermocouple wire, eventually, the interface depositing with a layer of crust (Farid, 2003). On this moment, the droplet turns into a scattered wet particle assembly and the evaporation continues until the particle moisture content reduces to an equilibrium with the drying air (D-E) (Handscorn et al., 2009). After that, the evaporation process finally stops and the nanoparticle is heated up to the equilibrium temperature (E-F).

The nature of heat transfer between plasmonic nanoparticle and water cannot be fully understood through the classical models and suggest collective effects including hot spots and electrons (Brongersma et al., 2015; Hogan et al., 2014; Richardson et al., 2009). This mechanism is extremely efficient because the heat fluxes from a large ensemble of nanoparticles resulting in water temperature a few orders of magnitude larger than the temperature induced by a single nanoparticle. In our experiment, plasmonic droplets have a small volume fluid with a high concentration of the particle number. This small volume delivers the generated heat to its water/air interface for vapor release in a shorter time. In this situation, rapid mixing and temperature equilibration inside the droplet can be expected and non-linearly optical depth is ignored. Thus, a collective heating effect of many nanoparticles dominate within the excitation volume, in particular, the particle assembly leads to a bulk heat distribution due to simultaneous light absorption and scattering (Fig. 10). This collective heating are controlled by two parameters: one that relates the morphology properties of the droplet and the other that characterizes the interparticle gap. We now explain the mechanism by modelling of a photo-excited droplet containing nanoparticles. The ratio between the collective temperature in the droplet center and the single-nanoparticle temperature can be estimated as $\delta = \frac{\Delta T_{collective}}{\Delta T_{surface\ of\ single\ particle}} \approx N_{NP,tot} r/R$, where, r and $R = D/2$ are the particle radius and the equivalent radius of droplet, and $N_{NP,tot}$ is the total number particle within the droplet (Baral et al., 2014; Govorov et al., 2006; Richardson et al., 2009). In our case,

the collective ratio is a large number $\delta \sim 45800$, since the nanoparticle density is $\sim 4.24 \times 10^{11}/\text{ml}$ for the droplet at $25 \mu\text{g}/\text{ml}$. This is the regime where the heating is intense due to its collective property. Therefore, a temperature amplification is input to the surrounding liquid, and the macroscale domain of temperature is increased, not just a local region around the gold nanoparticle. The small volume liquid thus can be triggered at relatively low optical intensities to the boiling point where steam releasing with high efficiency.

4. Conclusion

The nano/mesoscale engineering concept coupling plasmonic nanoparticles within a mesoscale droplet were demonstrated to be an efficient platform for solar water evaporation, leading to intense vapor production under a moderate optical density. The plasmon effect and highly active surfaces offered by the gold nanoparticles greatly improve photon absorption of solar energy. Even at a low mass concentration of gold particle $\sim 25 \mu\text{g}/\text{ml}$, the evaporation duration of the droplet can reduce by 36% compared to that of the base water droplet. The evaporation rate with particle concentration of 10 and $100 \mu\text{g}/\text{ml}$ are similar, which is slower than the droplet at $25 \mu\text{g}/\text{ml}$, indicating an optimal initial-particle-concentration exists. This discloses an effective approach to modify the optical and thermodynamic properties of the nanofluids. We also observed that shrinking of the droplet significantly enhances the surface evaporation. The surface evaporation rate increase with the increasing particle concentration, reaching an optimized value at a threshold concentration and then stable. The K value presenting a nonlinear property implies a complex heat-transfer physics. A collective energy absorption by multiple light scattering within the droplet accounts for the vapor generation. The heating intensity is related to the droplet morphology as well as the interparticle gap. This work provides a first study of solar evaporation of plasmonic droplets and the findings is significant important for further development of the plasmonic nanoheaters. Future studies on the interplay between plasmonics and nanoscale heat transfer are required for a thorough understanding of the beneath mechanism, which could have a far-reaching impact on the field.

Notes

The authors declare no competing financial interest.

Acknowledgements

The authors acknowledge the support from the Nature Science Foundation of China (51576002 and 51436004).

References

- Amjad, M., Raza, G., Xin, Y., Pervaiz, S., Xu, J., Du, X., Wen, D., 2017. Volumetric solar heating and steam generation via gold nanofluids. *Appl. Energy* 206, 393–400.
- Baffou, G., Polleux, J., Rigneault, H., Monneret, S., 2014. Super-heating and micro-bubble generation around plasmonic nanoparticles under cw illumination. *J. Phys. Chem. C* 118 (9), 4890–4898.
- Baffou, G., Quidant, R., Garcia de Abajo, F.J., 2010. Nanoscale control of optical heating in complex plasmonic systems. *ACS Nano* 4 (2), 709–716.
- Baral, S., Green, A.J., Livshits, M.Y., Govorov, A.O., Richardson, H.H., 2014. Comparison of vapor formation of water at the solid/water interface to colloidal solutions using optically excited gold nanostructures. *ACS Nano* 8 (2), 1439–1448.
- Berry, K.R., Dunklin, J.R., Blake, P.A., Roper, D.K., 2015. Thermal dynamics of plasmonic nanoparticle composites. *J. Phys. Chem. C* 119 (19), 10550–10557.
- Bertocchi, R., Karni, J., Kribus, A., 2004. Experimental evaluation of a non-isothermal high temperature solar particle receiver. *Energy* 29 (5–6), 687–700.
- Brongersma, M.L., Halas, N.J., Nordlander, P., 2015. Plasmon-induced hot carrier science and technology. *Nat. Nanotechnol.* 10 (1), 25–34.
- Chen, C., Li, Y., Song, J., Yang, Z., Kuang, Y., Hitz, E., Jia, C., Gong, A., Jiang, F., Zhu, J.Y., Yang, B., Xie, J., Hu, L., 2017. Highly flexible and efficient solar steam generation device. *Adv. Mater.* 29 (30).
- Chen, H., Shao, L., Ming, T., Sun, Z., Zhao, C., Yang, B., Wang, J., 2010. Understanding the photothermal conversion efficiency of gold nanocrystals. *Small* 6 (20), 2272–2280.
- Chen, R.-H., Phuoc, T.X., Martello, D., 2010. Effects of nanoparticles on nanofluid droplet evaporation. *Int. J. Heat Mass Transf.* 53 (19–20), 3677–3682.
- Chen, R.-H., Phuoc, T.X., Martello, D., 2011. Surface tension of evaporating nanofluid droplets. *Int. J. Heat Mass Transf.* 54 (11–12), 2459–2466.
- Deegan, R.D., Bakajin, O., Dupont, T.F., Huber, G., Nagel, S.R., Witten, T.A., 1997. Capillary flow as the cause of ring stains from dried liquid drops. *Nature* 389 (6653), 827–829.
- Deng, Z., Zhou, J., Miao, L., Liu, C., Peng, Y., Sun, L., Tanemura, S., 2017. The emergence of solar thermal utilization: solar-driven steam generation. *J. Mater. Chem. A* 5 (17), 7691–7709.
- Fang, Z., Zhen, Y.R., Neumann, O., Polman, A., Garcia de Abajo, F.J., Nordlander, P., Halas, N.J., 2013. Evolution of light-induced vapor generation at a liquid-immersed metallic nanoparticle. *Nano Lett.* 13 (4), 1736–1742.
- Farid, M., 2003. A new approach to modelling of single droplet drying. *Chem. Eng. Sci.* 58 (13), 2985–2993.
- Gao, M., Connor, P.K.N., Ho, G.W., 2016. Plasmonic photothermic directed broadband sunlight harnessing for seawater catalysis and desalination. *Energy Environ. Sci.* 9 (10), 3151–3160.
- Gerken, W.J., Thomas, A.V., Koratkar, N., Oehlschlaeger, M.A., 2014. Nanofluid pendant droplet evaporation: experiments and modeling. *Int. J. Heat Mass Transf.* 74, 263–268.
- Ghasemi, H., Ni, G., Marconnet, A.M., Loomis, J., Yerci, S., Miljkovic, N., Chen, G., 2014. Solar steam generation by heat localization. *Nat. Commun.* 5, 4449.
- Ghosh, S.K., Pal, T., 2007. Interparticle coupling effect on the surface plasmon resonance of gold nanoparticles: from theory to applications. *Chem. Rev.* 107 (11), 4797–4862.
- Govorov, A.O., Richardson, H.H., 2007. Generating heat with metal nanoparticles. *Nano Today* 2 (1), 30–38.
- Govorov, A.O., Zhang, W., Skeini, T., Richardson, H., Lee, J., Kotov, N.A., 2006. Gold nanoparticle ensembles as heaters and actuators: melting and collective plasmon resonances. *Nanoscale Res. Lett.* 1 (1), 84–90.
- Guo, A., Fu, Y., Wang, G., Wang, X., 2017. Diameter effect of gold nanoparticles on photothermal conversion for solar steam generation. *RSC Adv.* 7 (8), 4815–4824.
- Handscomb, C.S., Kraft, M., Bayly, A.E., 2009. A new model for the drying of droplets containing suspended solids. *Chem. Eng. Sci.* 64 (4), 628–637.
- Hentschel, M., Saliba, M., Vogelgesang, R., Giessen, H., Alivisatos, A.P., Liu, N., 2010. Transition from isolated to collective modes in plasmonic oligomers. *Nano Lett.* 10 (7), 2721–2726.
- Hogan, N.J., Urban, A.S., Ayala-Orozco, C., Pimpinelli, A., Nordlander, P., Halas, N.J., 2014. Nanoparticles heat through light localization. *Nano Lett.* 14 (8), 4640–4645.
- Jain, P.K., Huang, W., El-Sayed, M.A., 2007. On the universal scaling behavior of the distance decay of plasmon coupling in metal nanoparticle pairs: a plasmon ruler equation. *Nano Lett.* 7 (7), 2080–2088.
- Jain, P.K., Lee, K.S., El-Sayed, I.H., El-Sayed, M.A., 2006. Calculated absorption and scattering properties of gold nanoparticles of different size, shape, and composition: applications in biological imaging and biomedicine. *J. Phys. Chem. B* 110 (14), 7238–7248.
- Ji, X., Song, X., Li, J., Bai, Y., Yang, W., Peng, X., 2007. Size control of gold nanocrystals in citrate reduction: the third role of citrate. *J. Am. Chem. Soc.* 129 (45), 13939–13948.
- Jin, H., Lin, G., Bai, L., Amjad, M., Bandarra Filho, E.P., Wen, D., 2016a. Photothermal conversion efficiency of nanofluids: an experimental and numerical study. *Sol. Energy* 139, 278–289.
- Jin, H., Lin, G., Bai, L., Zeiny, A., Wen, D., 2016b. Steam generation in a nanoparticle-based solar receiver. *Nano Energy* 28, 397–406.
- John A. Duffie, W.A.B., 2013. *Solar Engineering of Thermal Processes*. Copyright 2013 by John Wiley & Sons.
- Kalogirou, S.A., 2004. Solar thermal collectors and applications. *Prog. Energy Combust. Sci.* 30 (3), 231–295.
- Khullar, V., Tyagi, H., Hordy, N., Otanicar, T.P., Hewakuruppu, Y., Modi, P., Taylor, R.A., 2014. Harvesting solar thermal energy through nanofluid-based volumetric absorption systems. *Int. J. Heat Mass Transf.* 77, 377–384.
- Kim, S.J., Bang, J.C., Buongiorno, J., Hu, L.W., 2007. Surface wettability change during pool boiling of nanofluids and its effect on critical heat flux. *Int. J. Heat Mass Transf.* 50 (19–20), 4105–4116.
- Langmuir, I., 1918. The evaporation of small spheres. *Phys. Rev.* 12 (5), 368–370.
- Lee, B.J., Park, K., Walsh, T., Xu, L., 2012. Radiative heat transfer analysis in plasmonic nanofluids for direct solar thermal absorption. *J. Sol. Energy Eng.* 134 (2), 021009.
- Lenert, A., Wang, E.N., 2012. Optimization of nanofluid volumetric receivers for solar thermal energy conversion. *Sol. Energy* 86 (1), 253–265.
- Lewis, N.S., 2016. Research opportunities to advance solar energy utilization. *Science* 351(6271), aad1920.
- Li, X., Xu, W., Tang, M., Zhou, L., Zhu, B., Zhu, S., Zhu, J., 2016. Graphene oxide-based efficient and scalable solar desalination under one sun with a confined 2D water path. *PNAS* 113 (49), 13953–13958.
- Liu, G., Xu, J., Wang, K., 2017. Solar water evaporation by black photothermal sheets. *Nano Energy* 41, 269–284.
- Liu, G.L., Kim, J., Lu, Y., Lee, L.P., 2006. Optofluidic control using photothermal nanoparticles. *Nat. Mater.* 5 (1), 27–32.
- Loeb, S., Li, C., Kim, J.H., 2018. Solar photothermal disinfection using broadband-light absorbing gold nanoparticles and carbon black. *Environ. Sci. Technol.* 52 (1), 205–213.
- Lombard, J., Biben, T., Merabia, S., 2014. Kinetics of nanobubble generation around overheated nanoparticles. *Phys. Rev. Lett.* 112 (10), 105701.
- Lombard, J., Biben, T., Merabia, S., 2017. Threshold for vapor nanobubble generation around plasmonic nanoparticles. *J. Phys. Chem. C* 121 (28), 15402–15415.
- Metwally, K., Mensah, S., Baffou, G., 2015. Fluence threshold for photothermal bubble generation using plasmonic nanoparticles. *J. Phys. Chem. C* 119 (51), 28586–28596.
- Ming, T., Kou, X., Chen, H., Wang, T., Tam, H.L., Cheah, K.W., Chen, J.Y., Wang, J., 2008. Ordered gold nanostructure assemblies formed by droplet evaporation. *Angew. Chem.* 47 (50), 9685–9690.
- Neumann, O., Feronti, C., Neumann, A.D., Dong, A., Schell, K., Lu, B., Kim, E., Quinn, M., Thompson, S., Grady, N., Nordlander, P., Oden, M., Halas, N.J., 2013a. Compact solar autoclave based on steam generation using broadband light-harvesting nanoparticles. *PNAS* 110 (29), 11677–11681.
- Neumann, O., Urban, A.S., Day, J., Lal, S., Nordlander, P., Halas, N.J., 2013b. Solar vapor generation enabled by nanoparticles. *ACS Nano* 7 (1), 42–49.
- Ni, G., Miljkovic, N., Ghasemi, H., Huang, X., Boriskina, S.V., Lin, C.-T., Wang, J., Xu, Y., Rahman, M.M., Zhang, T., Chen, G., 2015. Volumetric solar heating of nanofluids for direct vapor generation. *Nano Energy* 17, 290–301.
- Otanicar, T.P., Phelan, P.E., Prasher, R.S., Rosengarten, G., Taylor, R.A., 2010. Nanofluid-based direct absorption solar collector. *J. Renewable Sustainable Energy* 2 (3), 033102.
- Richardson, H.H., Carlson, M.T., Tandler, P.J., Hernandez, P., Govorov, A.O., 2009. Experimental and theoretical studies of light-to-heat conversion and collective heating effects in metal nanoparticle solutions. *Nano Lett.* 9 (3), 1139–1146.
- Roxworthy, B.J., Bhuiya, A.M., Vanka, S.P., Toussaint Jr., K.C., 2014. Understanding and controlling plasmon-induced convection. *Nat. Commun.* 5, 3173.
- Sadek, C., Schuck, P., Fallourd, Y., Pradeau, N., Le Floch-Fouéré, C., Jeantet, R., 2014. Drying of a single droplet to investigate process–structure–function relationships: a review. *Dairy Sci. Technol.* 95 (6), 771–794.
- Shang, W., Deng, T., 2016. Solar steam generation: steam by thermal concentration. *Nat. Energy* 1 (9), 16133.
- Swinehart, D.F., 1962. The Beer-Lambert Law. *J. Chem. Educ.* 39 (7), 333.
- Thiruganasambandam, M., Iniyar, S., Goic, R., 2010. A review of solar thermal technologies. *Renew. Sustain. Energy Rev.* 14 (1), 312–322.
- Tian, L., Luan, J., Liu, K.K., Jiang, Q., Tadepalli, S., Gupta, M.K., Naik, R.R., Singamaneni, S., 2016. Plasmonic biofoam: a versatile optically active material. *Nano Lett.* 16 (1), 609–616.
- Wang, X., He, Y., Cheng, G., Shi, L., Liu, X., Zhu, J., 2016. Direct vapor generation through localized solar heating via carbon-nanotube nanofluid. *Energy Convers. Manage.* 130, 176–183.
- Wang, X., He, Y., Liu, X., Shi, L., Zhu, J., 2017. Investigation of photothermal heating enabled by plasmonic nanofluids for direct solar steam generation. *Sol. Energy* 157, 35–46.
- Wang, Y., Zaytsev, M.E., The, H.L., Eijkel, J.C., Zandvliet, H.J., Zhang, X., Lohse, D., 2017. Vapor and gas-bubble growth dynamics around laser-irradiated, water-immersed plasmonic nanoparticles. *ACS Nano* 11 (2), 2045–2051.
- Wei, Y., Deng, W., Chen, R.-H., 2016. Effects of insoluble nano-particles on nanofluid droplet evaporation. *Int. J. Heat Mass Transf.* 97, 725–734.
- Weinstein, L., Kraemer, D., McEnaney, K., Chen, G., 2014. Optical cavity for improved performance of solar receivers in solar-thermal systems. *Sol. Energy* 108, 69–79.
- Weinstein, L.A., Loomis, J., Bhatia, B., Bierman, D.M., Wang, E.N., Chen, G., 2015. Concentrating solar power. *Chem. Rev.* 115 (23), 12797–12838.
- Zhao, P., Li, N., Astruc, D., 2013. State of the art in gold nanoparticle synthesis. *Coord. Chem. Rev.* 257 (3–4), 638–665.
- Zhou, L., Tan, Y., Wang, J., Xu, W., Yuan, Y., Cai, W., Zhu, S., Zhu, J., 2016. 3D self-assembly of aluminum nanoparticles for plasmon-enhanced solar desalination. *Nat. Photonics* 10 (6), 393–398.
- Zhu, M., Li, Y., Chen, F., Zhu, X., Dai, J., Li, Y., Yang, Z., Yan, X., Song, J., Wang, Y., Hitz, E., Luo, W., Lu, M., Yang, B., Hu, L., 2017. Plasmonic wood for high-efficiency solar steam generation. *Adv. Energy Mater.* 1701028.
- Zielinski, M.S., Choi, J.W., La Grange, T., Modestino, M., Hashemi, S.M., Pu, Y., Birkhold, S., Hubbell, J.A., Psaltis, D., 2016. Hollow mesoporous plasmonic nanoshells for enhanced solar vapor generation. *Nano Lett.* 16 (4), 2159–2167.